Nanoscale

PAPER

View Article Online
View Journal | View Issue

Cite this: *Nanoscale*, 2019, **11**, 22387

Nontoxic amphiphilic carbon dots as promising drug nanocarriers across the blood–brain barrier and inhibitors of β-amyloid†

Yiqun Zhou,[a] Piumi Y. Liyanage,[a] Dinesh Devadoss,[b] Linda Rebeca Rios Guevara,[a] Ling Cheng,[a] Regina M. Graham,[c] Hitendra S. Chand,[b] Abdulrahman O. Al-Youbi,[d] Abdulaziz S. Bashammakh,[d] Mohammad S. El-Shahawi[d] and Roger M. Leblanc *[a]

The blood–brain barrier (BBB) is a main obstacle for drug delivery targeting the central nervous system (CNS) and treating Alzheimer's disease (AD). In order to enhance the efficiency of drug delivery without harming the BBB integrity, nanoparticle-mediated drug delivery has become a popular therapeutic strategy. Carbon dots (CDs) are one of the most promising and novel nanocarriers. In this study, amphiphilic yellow-emissive CDs (Y-CDs) were synthesized with an ultrasonication-mediated methodology using citric acid and *o*-phenylenediamine with a size of 3 nm that emit an excitation-independent yellow photoluminescence (PL). The content of primary amine and carboxyl groups on CDs was measured as 6.12×10^{-5} and 8.13×10^{-3} mmol mg^{-1}, respectively, indicating the potential for small-molecule drug loading through bioconjugation. Confocal image analyses revealed that Y-CDs crossed the BBB of 5-day old wild-type zebrafish, most probably by passive diffusion due to the amphiphilicity of Y-CDs. And the amphiphilicity and BBB penetration ability didn't change when Y-CDs were coated with different hydrophilic molecules. Furthermore, Y-CDs were observed to enter cells to inhibit the overexpression of human amyloid precursor protein (APP) and β-amyloid (Aβ) which is a major factor responsible for AD pathology. Therefore, data suggest that Y-CDs have a great potential as nontoxic nanocarriers for drug delivery towards the CNS as well as a promising inhibiting agent of Aβ-related pathology of the AD.

Received 23rd September 2019,
Accepted 12th November 2019

DOI: 10.1039/c9nr08194a

rsc.li/nanoscale

1. Introduction

Alzheimer's disease (AD) is an irreversible and progressive brain disorder.[1] It gradually influences person's activity by impairing memory and other cognitive abilities. Also it is an epidemic amongst the elderly population aged more than 65 years old and it rapidly worsens the neurologic activities over time.[2] According to the statistics of National Institute on Aging, more than 5.5 million Americans may have dementia caused by AD. And Alzheimer's Association claims that it is the sixth leading cause of death in the United States.[3] Therefore, it is of great significance to prevent AD and treat those patients who are suffering the memory loss and behavioral disorder it brings. Although there is still no cure, the current treatment options including chemotherapy have shown the promise to slow down its progression by specifically targeting certain AD contributors.[4] While the roles of tau protein, acetylcholinesterase level and reactive oxygen species (ROS) in its progression have all been validated and studied, amyloid plaque formed by β-amyloid (Aβ) is considered as the major pathology of AD.[5–7] However, the focus of AD treatment is still on blocking or disrupting the formation of amyloid plaque but numerous therapeutics fail the clinical trial partly due to the limited capability to cross the blood–brain barrier (BBB).[8]

BBB is the main protection mechanism of the central nervous system (CNS) that shields the brain from blood-borne pathogens and other unwanted molecules.[9] However, it also becomes a main obstacle for drug delivery to the brain. More than 90% of small molecules are unable to pass the BBB while almost 100% of large molecules cannot penetrate the BBB by passive diffusion.[10] Molecules that have the potential to cross the BBB through passive diffusion must meet the character-

[a]*Department of Chemistry, University of Miami, Coral Gables, FL 33146, USA. E-mail: rml@miami.edu*
[b]*Department of Immunology and Nano-Medicine, Florida International University, Miami, FL 33199, USA*
[c]*Department of Neurological Surgery, Miller School of Medicine, University of Miami, Miami, Florida 33136, USA*
[d]*Department of Chemistry, King Abdulaziz University, P.O. Box 80200, Jeddah 21589, Kingdom of Saudi Arabia*

† Electronic supplementary information (ESI) available. See DOI: 10.1039/c9nr08194a

istics such as small size, low hydrophilicity and surface charge. In addition, active transport including receptor-, absorption-mediated endocytosis and carrier-mediated transport is another route for most large molecules to overcome the BBB.[11] For example, due to the overexpression of transferrin and folic acid receptors on the BBB, transferrin and folic acid can pass the BBB through a receptor-mediated endocytosis.[11] In recent years, nanoparticle-mediated drug delivery has proven to be a relatively noninvasive alternative to conventional approaches such as temporary disruption of the tight junction between endothelial cells, which cause the damage to the integrity of the BBB and result in an uncontrolled influx of unwanted molecules into the CNS.[12] Nanoparticles are better drug carriers due to their many advantageous characteristics such as small size, large surface area to volume ratio, and tunable surface, which provide favorable conditions for drug conjugation and delivery.[13]

Amongst all nanoparticle species, carbon dots (CDs) are one of the most promising drug nanocarriers. Compared with gold, silver, or traditional quantum dots (QDs), CDs are novel carbon-based nanoparticles with relatively no toxicity and high biocompatibility. Also, compared to liposomes, CDs are smaller, with their size ranging between 1–10 nm. In contrast to carbon nanotubes, CDs are easier to synthesize, and they have large surface area to volume ratio which enhances the drug loading capacity for drug delivery. Despite of these superior properties, CDs are characterized for their high photoluminescence (PL). Considering CDs' excellent PL, CDs have been widely applied in sensing and bioimaging.[14] Compared with many known metal-based photocatalyst materials, CDs will not pose the risk of secondary water contamination due to their nontoxicity and good biocompatibility.[15] In addition, CDs have been observed to inhibit the fibrilization of protein and Aβ, which show a great potential for the treatment of AD.[16,17] Nonetheless, those work remains in the *in vitro* level. CDs have another well-known property, high water-dispersity, which is beneficial for conducting homogeneous photocatalysis or partial drug delivery. However, to cross the BBB, as was mentioned before, nanocarrier should be less hydrophilic or amphiphilic. Few reports have shown CDs with the ability to cross the BBB without conjugation with transferrin or the help of transporters such as LAT1 and GLUT1.[18] Also, most reported CDs have short-emissive PL such as blue PL. Regardless of their high fluorescence quantum yield, blue emission interferes with the autofluorescence of some tissues or organs in animal studies, which makes drug difficult to track. In contrast, long-emissive CDs would not demonstrate this interference, making such CDs more desirable. According to recent reports, the isomers of phenylenediamine have been widely applied to successfully synthesize CDs with long emission wavelengths with hydrothermal/solvothermal methods.[19,20] However, the obtained CDs cannot often disperse into water,[21] which greatly limits their applications.

Herein, to mitigate these issues, novel amphiphilic yellow-emissive CDs (Y-CDs) were developed with citric acid and *o*-phenylenediamine dissolved in water *via* an ultrasonication approach. Following intravascular injection, Y-CDs were localized in the spinal cord central canal of 5-day old wild-type zebrafish. Since zebrafish (*Danio rerio*) is a relatively complicated vertebrate species with a high degree of physiological and genetic homology to humans, they are considered as an excellent model for the BBB of human.[22] The obtained Y-CDs showed the capability to cross the BBB and the potential as drug nanocarriers. Zebrafish were used as an *in vivo* model considering several advantages over the mice models: (1) zebrafish don't require large space and also they are more cost-effective to keep than mice colonies;[23] (2) adult zebrafish breed approximately every 10 days and can lay 50 to 300 eggs at a time.[24] In contrast, mice in general produce a litter of up to 10 pups but can only bear around five litters for a whole lifetime. Therefore, zebrafish are more helpful because they can produce a large number of offspring to help repeat experiments with multiple replicates to obtain robust results; (3) zebrafish embryos and larvae are nearly transparent, which allows researchers to observe the real-time development of tissues and any fluorescently labeled activity in zebrafish body.[25] In contrast, mouse embryos are not translucent and naturally develop inside the mother, so it is not possible to observe live embryo development and fluorescently labeled activity as seen in zebrafish. Therefore, with all the advantages taken into consideration, zebrafish model was employed in this study.

In addition, the toxicity of Y-CDs was tested in relevant mammalian cell lines. The bare Y-CDs were also used to test their efficacy in inhibiting the Aβ plaques formation. Although previously, Li *et al.* have shown that CDs prepared from carbon nanopowder could cross the BBB by conjugation with transferrin while inhibiting protein fibrillation, experimental evidence demonstrated that the bare CDs could not pass the BBB.[23] The detailed analysis further revealed that the CDs used had abundant hydrophilic groups including –COOH and C═O, and had spherical diameter of 6 nm, which makes it very challenging for passive diffusion of these CDs through the BBB. Therefore, in comparison to other established work, the significance of our work includes (1) the use of long-emissive Y-CDs as *in vivo* drug nanocarriers to avoid interference of autofluorescence; (2) cross the BBB using Y-CDs by passive diffusion; (3) inhibition of Aβ plaques formation by reducing Aβ secretion in cells for the promising treatment of AD.

2. Experimental

Materials

Citric acid (99.5–100%) was ordered from VWR (West Chester, PA, USA). *o*-Phenylenediamine (99.5%), EDC, NHS (97.0%), 3-amino-1-propanol (99.0%) and diethanolamine (DEA) (99.9%) were all purchased from Sigma-Aldrich (St Louis, MO, USA). The deionized water applied was purified using a Modulab 2020 water purification system acquired from Continental Water System Corporation (San Antonio, TX, USA). It had a pH of 6.62 ± 0.30 at 25.0 ± 0.5 °C. The GE Healthcare

Sephacryl S-300 (Uppsala, Sweden) was used in the size exclusion chromatography (SEC) as the stationary matrix. In the end, all the chemicals were used without any further treatment.

Instrumentations

The UV/vis absorption spectroscopic date of Y-CDs was obtained by using a Cary 100 UV/vis spectrophotometer (Santa Clara, CA, USA) and a 1 cm quartz cuvette. A Fluorolog spectrometer (Horiba Jobin Yvon) (Irvine, CA, USA) was applied to record the spectrum of fluorescence. The slit width was 5 nm for both excitation and emission. FTIR spectrum was measured with a PerkinElmer FTIR (Frontier) spectrometer (Waltham, MA, USA) by using an attenuated total reflection (ATR) technique with air as the background. A nano series Malvern Zetasizer (Westborough, MA, USA) was used to perform the zeta potential measurements. TEM images were acquired with the use of a JEOL 1200× TEM (Peabody, MA, USA). Prior to the TEM measurement, 5 min ultrasonication was conducted with the use of a Branson 1510 ultrasonic cleaner (Gaithersburg, MD, USA) to well disperse Y-CDs in water and avoid aggregation. To conduct the TEM measurement, a drop of Y-CDs aqueous dispersion treated by ultrasonication was deposited on a carbon-coated copper grid and dried with air before the TEM screening.

Synthesis of Y-CDs

Synthesis of Y-CDs requires 0.02 g citric acid as a carbon source and 0.28 g *o*-phenylenediamine as a N-dopant in a molar ratio of 1 : 25 which were completely dissolved in 10 mL deionized H_2O mediated by 5 min ultrasonication at a frequency of 42 kHz. Then the ultrasonication bath was further applied to sonicate the mixture for another 1 h at a frequency of 42 kHz. The whole ultrasonication process was protected by argon gas. After 1 h, an orange aqueous dispersion was obtained exhibiting a yellow PL emission under the excitation of UV light (365 nm). After a series of purification procedures that include filtration of the unreacted *o*-phenylenediamine in the ice bath and SEC to remove fluorophores in smaller size, Y-CDs remained in water. After lyophilization, Y-CDs were eventually obtained as an orange powder.

Quantification of primary amine and carboxyl groups on Y-CDs

The primary amine group was quantified by a fluorescence analysis using fluorescamine assay based on our previous work.[26] 2 mg of Y-CDs was added into a 2 mL volumetric flask which was filled up with 1× PBS buffer solution. Then 50 μL CDs dispersion was transferred to a 5 mL volumetric flask together with 0.5 mg fluorescamine and the flask was filled with the same 1× PBS buffer solution. According to the linear relationship between the molarity of primary amine group and the fluorescence intensity using 1,2-ethylenediamine (EDA) as a standard, the intensity of fluorescence generated upon the addition of fluorescamine into Y-CDs aqueous dispersion was interpolated into the equation of linear relationship and the amount of primary amine group was measured on 2 mg of Y-CDs.

Meanwhile, the quantification of carboxyl group on the surface of Y-CDs was achieved by a classic acid–base titration. 1 mg mL^{-1} of Y-CDs stock aqueous dispersion was prepared and then diluted to 0.02 mg mL^{-1}. Then a volume of 50 mL of this diluted sample was titrated with 0.005 mol L^{-1} NaOH solution using phenolphthalein as the visual indicator. The titration was conducted slowly until the pink color is stable for over 3 min after the addition of NaOH in Y-CDs aqueous dispersion. Then the volume of NaOH solution was recorded for the calculation of the amount of carboxyl groups on Y-CDs.

Coating of Y-CDs

10 mg of Y-CDs and 25 mg of EDC were each dispersed or dissolved in 2 mL of PBS (pH 7.4), mixed together and stirred for 30 min. Then 15 mg of NHS was dissolved in 2 mL of PBS, added to the solution and stirred for another 30 min. 10 mg of 3-amino-1-propanol or 13 mg DEA was dissolved in PBS, added to the solution, and stirred overnight. After one night, the solution was transferred into the SEC column to separate conjugate from precursors. Then the first yellow-emissive eluent was collected and processed by lyophilization to get powders.

Zebrafish injection and bioimaging

Wild-type zebrafish at 5 days after fertilization were obtained from the Zebrafish Core Facility at University of Miami. 0.1 mg mL^{-1} Y-CDs aqueous dispersion was injected into the heart of zebrafish previously anesthetized by tricaine. After 10 min, the injected zebrafish were subjected for observation under a Leica SP5 confocal microscope under white light and excitation at 405 nm (for Y-CDs). The animal care protocol for all procedures used in this study was approved by the University of Miami Animal Care and Use Committee and complies with the guidelines of the National Science Foundation.

Cell culture and bioimaging

Pediatric glioblastoma cell lines (SJGBM2, CHLA200) and human embryonic kidney cell line (HEK293) were obtained from Children's Oncology Group, Lubbock, TX and American Type Culture Collection, Manassas, VA, USA, respectively. All above cell lines were cultured in RPMI-1640 media which was obtained from ThermoFisher Scientific, Waltham, MA, USA. The RPMI-1640 was pre-supplemented with 10% fetal bovine serum (FBS) and 1% penicillin/streptomycin (both from Gemini Biosciences, West Sacramento, CA) before using for culturing. The cultured cells were maintained in incubation at 37 °C with 5% CO_2. Dulbecco's modified Eagle's medium with 10% fetal bovine serum, 2 mM L-glutamine, 100 μg ml^{-1} penicillin, and 100 μg ml^{-1} streptomycin was used to culture the Chinese hamster ovary (CHO) cells that stably overexpress human amyloid precursor protein-751 (APP-751).

Cell viability was tested with the CellTiter 96® AQueous One Solution Cell Proliferation Assay (MTS) (Promega Madison, WI) using the two cell lines SJGBM2 and CHLA200. 96-Well plates were used for cell plating at a density of 0.5 ×

10^4 cells per well in a volume of 100 μL RPMI and incubated for 24 h before treating with Y-CDs of different concentrations (10, 1 and 0.1 μM) dispersed in another 100 μl RPMI. The cell plates were incubated for 72 hours before measuring for cell viability using MTS assay. For the viability assessment, the absorbances were measured at 490 nm using BoiTek Synergy HT plate reader. For CHO cell viability and Aβ monomers quantification, the cells were grown in 6-well plates while for the cellular uptake and APP expression studies the cells were grown in Lab-Tek Chamber slides until 80% confluence. Then cells were treated with Y-CDs in different concentrations such as 0, 0.1, 1 and 10 μM for 24 or 48 h. The viability was determined by staining the cells with the Trypan blue stain.

For the microscope imaging of cells, the SJGBM2 and HEK293 cells were used. The cells were first plated in wells containing FBS coated coverslips and incubated for 48 hours before treating with 50 μg ml^{-1} Y-CDs in RPMI for another 24 h. PBS solution was used to wash away any residues from the cells before fixing them with 4% paraformaldehyde at room temperature. Finally, these coverslips were mounted on to glass slides for bioimaging using an Olympus FV1000 confocal microscope.

Immunofluorescence analysis for APP

Briefly, after 24 h treatment of Y-CDs, cells were first fixed with 4% paraformaldehyde and rinsed with 0.05% Brij-35 in PBS (pH = 7.4). Nonspecific binding was blocked with blocking solution that contains 3% BSA, 1% gelatin, and 1% normal donkey serum with 0.1% of both Triton X-100 and saponin. Then cells were incubated with the primary antibody of APP (Novus, a biotechne brand, US) and stained with streptavidin-Alexa647. For nuclei visualization the cells were stained with 4′,6-diamidino-2-phenylindole (DAPI) containing Fluormount-G (SouthernBiotech, Birmingham, AL). Immunofluorescent images were captured with a BZX700 Microscopy system.

Aβ ELISA assay

Human Aβ 40 levels were obtained using an ELISA kit (Immuno-Biological laboratories Inc., Minneapolis, MN, USA) following the manufacturer's protocol. Briefly, cell culture media from control and Y-CDs treated (24 h) were added into the assay wells pre-coated with anti-human Aβ and incubated overnight at 4 °C. Then it was incubated with HRP-conjugated secondary antibody at 4 °C. After an hour, tetramethylbenzidine was added and incubated at room temperature for 30 min. In the end, this reaction was stopped by adding stop solution and the formed color reagent was measured at 450 nm against a reagent blank. Aβ levels were calculated pg ml^{-1} of media and expressed as percentage change from controls.

3. Results and discussion

Synthesis and characterization of Y-CDs

In this study, the synthesis of Y-CDs didn't apply traditional harsh synthetic approaches such as hydrothermal/solvothermal or even microwave.[15,27] Instead, we used ultrasonication as a relatively mild reaction condition. However, ultrasonication is not the first time to report. Ma *et al.* reported a N-doped CD preparation *via* ultrasonication with aqueous ammonia and glucose as precursors in 2012.[28] According to their hypothesis, Y-CDs preparation mediated by ultrasonication was related to the formation and collapse of tiny vacuum bubbles that resulted from alternating high and low pressures in the reaction medium. And the cavitation would lead to high-speed impinging liquid jets, deagglomeration, and intense hydrodynamic shear forces. All of them could further carbonize the intermediate earlier generated by the dehydration of citric acid and *o*-phenylenediamine caused by ultrasonication.

Regarding characterization, the spectrum of UV/vis absorption (Fig. 1a) of Y-CDs revealed four peaks, which can be assigned to C=C (235 nm), C=N (255 nm), C=O (285 nm) conjugates and absorption cross section of NO_2 (421 nm) on Y-CDs,[29,30] respectively. The fluorescence emission spectrum (Fig. 1b) as well as its normalized spectrum in the inset demonstrated that Y-CDs have excitation-independent PL emission. And the maximum excitation and emission wavelengths are 400 and 562 nm, respectively. From the Fourier-transform infrared (FTIR) spectrum in Fig. 1c we could observe that peaks at 3276 cm^{-1} can be assigned to N–H or O–H group, which contribute to the water-dispersity of Y-CDs.[27,31] Meanwhile, peaks at 1620, 1500 and 1273 cm^{-1} correspond to N–H, C=O or C=C, and C–C or C–N stretches,[27] respectively. Among them, C=C conjugate structure, previously confirmed by UV/vis absorption and fluorescence emission spectra, together with C–C plays an important part in the hydrophobicity of Y-CDs. Furthermore, $-NH_2$ and –COOH have been quantified following a fluorescence analysis and an acid–base titration as 6.12×10^{-5} and 8.13×10^{-3} mmol mg^{-1}, respectively. As for the particle size, TEM images in Fig. 1d illustrated that the size of Y-CDs on average is 3.4 ± 1.0 nm. Therefore, various characterizations have demonstrated Y-CDs have long-emissive PL and small size.

Crossing the BBB with Y-CDs

Zebrafish are genetically similar to humans and about 70% of genes related to human diseases have functional homologs in zebrafish.[32] Therefore, it has become one of the most popular animal models for studying developmental processes and human disorders including hematological, heart, muscle, kidney, ocular and CNS disorders.[33,34] In terms of CNS disorder, many studies have applied zebrafish as a model system for the treatment of behavioral, neurological and neurodegenerative diseases such as Parkinson's, Huntington's, and Alzheimer's diseases.[35,36] And those studies have succesfully identified the orthologs of the major disease-related genes in zebrafish.[37,38] In addition, zebrafish have also been widely utilized in recent years to seek for the neuroactive drugs through behavioral screening.[39,40] The process of searching for new drugs to alleviate psychiatric and CNS disorders is a challenging, and because *in vitro* studies cannot predict

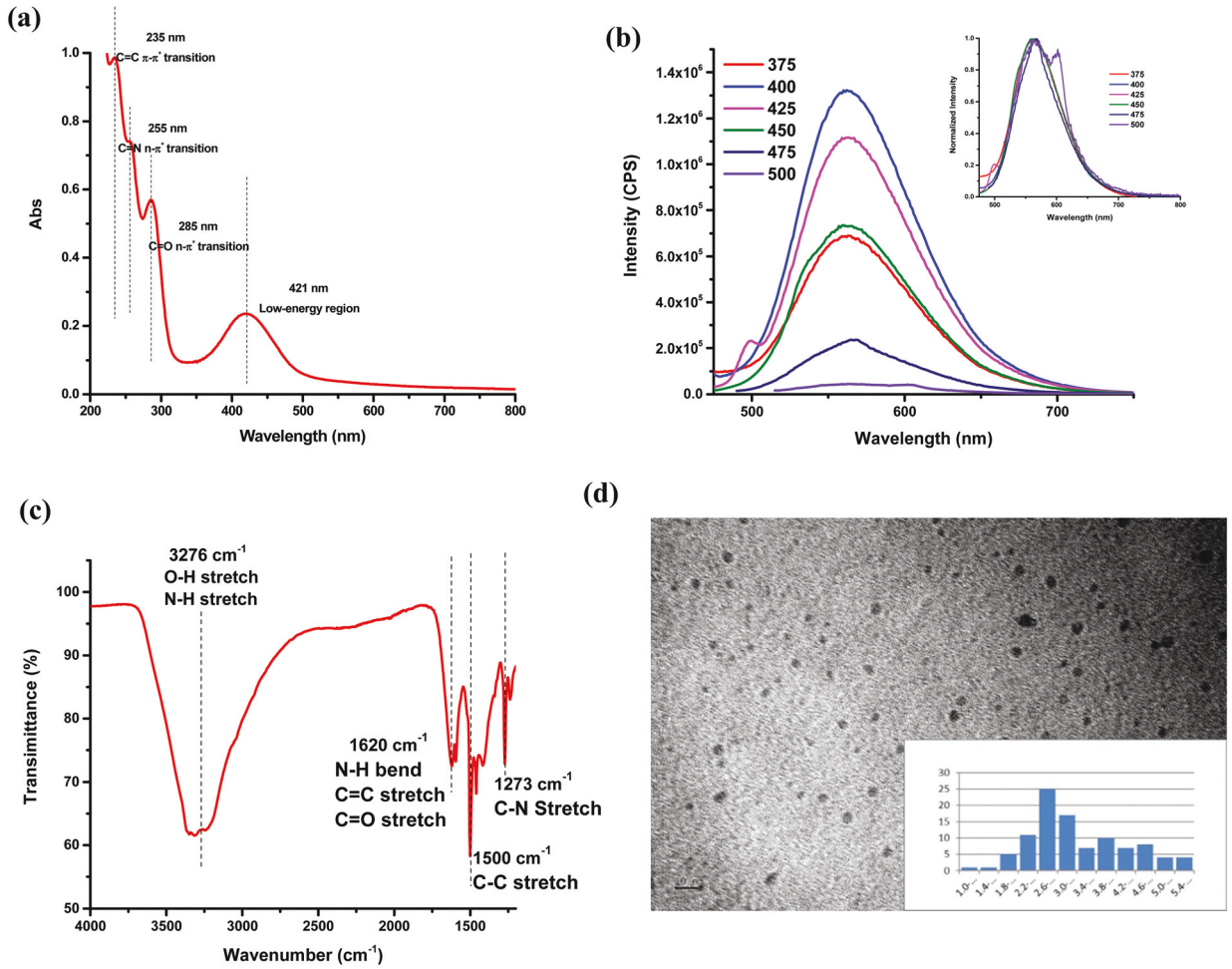

Fig. 1 Characterization of Y-CDs. (a) The UV/vis absorption spectrum measured with a 1 cm quartz cuvette (concentration: 0.025 mg mL^{-1}); (b) the fluorescence spectrum measured with a 1 cm quartz cuvette (concentration: 0.025 mg mL^{-1}) (inset is the normalized fluorescence spectrum); (c) FTIR spectrum with air as the background; (d) TEM image and size distribution histogram (inset).

therapeutic effect in *in vivo* test, the use of zebrafish becomes more necessary and convincing.[38] Furthermore, except for CDs, various biocompatible nanomaterials such as carbon nanotubes, graphene quantum dots and gold nanoparticles have been observed by Ke and coworkers as effective nanomedicines with or without surface modification to prevent and treat diverse human amyloid diseases with zebrafish as an *in vivo* model.[41–43] For instance, they reported when the amyloid fragments (b_a) of β-lactoglobulin, a whey protein, were deposited on the surface of carbon nanotubes, b_a sequestered human islet amyloid polypeptide (IAPP), a hallmark of type 2 diabetes exposed to zebrafish embryos through functional-pathogenic double-protein coronae.[42] And the b_a-coated carbon nanotubes removed the toxic IAPP species from zebrafish, which was confirmed by the assay of zebrafish embryonic development, studies of cell morphology, hatching, and survival and oxidative stress suppression.[42] Moreover, the b_a-coated carbon nanotubes also exhibited high efficacy against the toxicity of Aβ exposed to zebrafish embryos,[42] which demonstrate a broad applicability of the b_a-coated carbon nanotubes in the treatment of human amyloid diseases and the efficiency of zebrafish as a *in vivo* model.

As an important protection mechanism of the CNS, the BBB restricts the passage of most molecules which include the drugs used to treat the CNS-related diseases.[10] In order to improve the drug delivery across the BBB, diverse strategies have been employed such as neurosurgery and temporary disruption of the tight junctions by osmotic pressure, microbubbles or ultrasound.[44–47] However, these conventional therapeutic approaches pose risk to the integrity of BBB and the damage of structure may allow numerous unwanted toxins and molecules into the CNS.[48] Meanwhile, nanoparticle-mediated drug delivery targeting the BBB emerges as a relatively mitigatory approach and it has many advantages, which include non-invasiveness, long-term stability, ease of preparation, high targeting efficiency and controllability to load and release drugs after transverse of the BBB.[49,50] In our previous work, we have summarized various nanoparticles which have been employed for the drug delivery across the BBB.[10] Among

them, CDs are rather new in this area but have shown a great potential as drug nanocarriers.

Therefore, to examine whether Y-CDs can cross the BBB, 0.1 mg mL^{-1} Y-CDs aqueous dispersion was injected into the heart of 5-day wild-type zebrafish. Under the excitation of 405 nm, the confocal image (Fig. 2) in comparison to the control shows that Y-CDs can cross the BBB and show up in the central canal of spinal cord. As to the mechanism of Y-CDs across the BBB, since the precursor didn't involve transferrin or folic acid, whose receptors are overexpressed on the BBB, the mechanism of Y-CDs passing the BBB could not be a receptor-mediated endocytosis. And since the precursors were not composed of tryptophan or glucose, which could cross the BBB with unique transporter proteins, Y-CDs overcoming the BBB could not be due to the carrier-mediated transport. However, it may benefit from many unique properties of Y-CDs such as small size (3.4 ± 1.0 nm) and low zeta potential (−15.3 mV). In addition, Y-CDs have shown a solvent effect,[30] which indicates that Y-CDs can also disperse in many different organic solvents and display distinct PL properties. Therefore, it suggests the amphiphilicity of such CDs, which mediates the drug delivery through passive diffusion.

The mechanism hypothesis of drug delivery through passive diffusion was confirmed by soaking 5-day wild-type zebrafish (number of zebrafish applied: 10) in Y-CDs aqueous dispersion. 12 hours later, yellow fluorescence was exhibited in the skin, intestine, blood, liver, brain and spinal cord, which is shown in Fig. S1 in ESI† and has been exhibited in one of our previous publications.[51] In comparision, two other types of CDs were prepared as described with either carbon nanopowder or bovine serum albumin (BSA) as precursor.[16,52] However, we didn't observe the same effect when zebrafish (5-day, wild-type, number: 10) were soaked in the aqueous dispersion of these two types of CDs (Fig. S2 in ESI†). In comparison, the three CDs shared similar zeta potential and average particle size, which have been revealed by their zeta potential values (Table 1 in ESI†), TEM images (Fig. S3 in ESI†) and particle size analysis (Table 2 in ESI†). The major difference resides in the hydrophilicity or polarity of CDs. As was mentioned previously, Y-CDs are amphiphilic while the other two types of CDs are highly hydrophilic, which prevents these two types of CDs penetrating the lipophilic basement membrane of the BBB. Therefore, Fig. S1 in ESI† reveals a unique capability of Y-CDs to permeate into zebrafish by passive diffusion. In addition, the soaking experiment suggests the low hydrophilicity is a prerequisite for the penetration of the BBB.

Furthermore, in order to illustrate the importance of amphiphilicity of Y-CDs in penetrating the BBB, we performed two parallel experiments by separately coating Y-CDs with two hydrophilic molecules, 3-amino-1-propanol and DEA *via* amidation reactions in order to increase the hydrophilicity of Y-CDs. After lyophilization, both coated Y-CDs powders were characterized by fluorescence emission and FTIR spectroscopies to confirm the success of conjugations. According to the fluorescence emission spectra shown in Fig. S4 in ESI,† after conjugation with 3-amino-1-propanol or DEA, the PL emission is still excitation-independent. However, even though the emission peak at 562 nm barely changes, the maximum excitation wavelength has shifted from 400 to 425 nm after both conjugations. In addition, both FTIR spectra in Fig. S4 in ESI† clearly reveal the difference of conjugates and their precursors especially by the additional peaks at 2926–2827 cm^{-1} which is identified as the C–H stretch of 3-amino-1-propanol or DEA. Thus, both conjugations were confirmed with the change of structure and optical property of Y-CDs before and after conjugation. However, as one of the most attractive features of Y-CDs, the amphiphilicity was not changed through conjugation with hydrophilic molecules, which was confirmed with

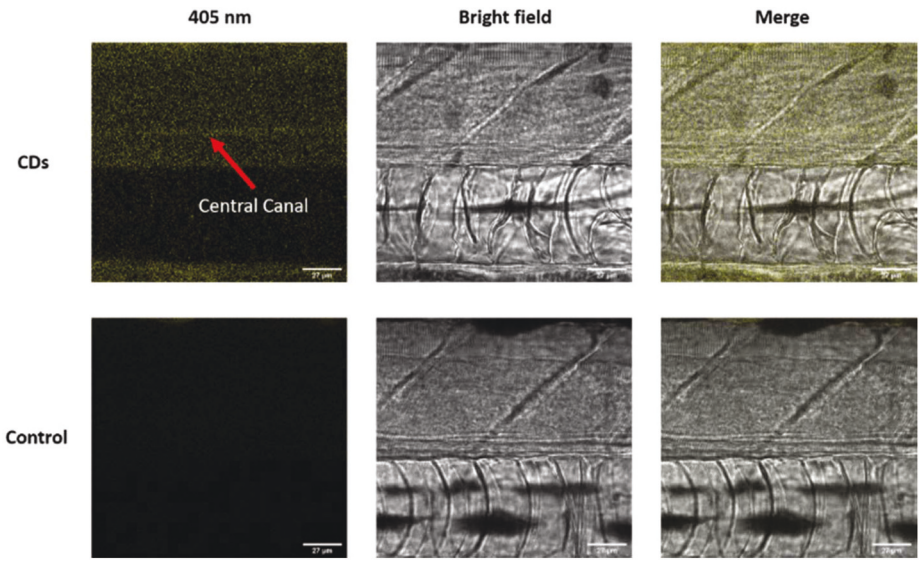

Fig. 2 Confocal images of Y-CDs aqueous dispersion (0.1 mg mL^{-1}) across the BBB. The red arrow indicates the central canal of spinal cord of zebrafish.

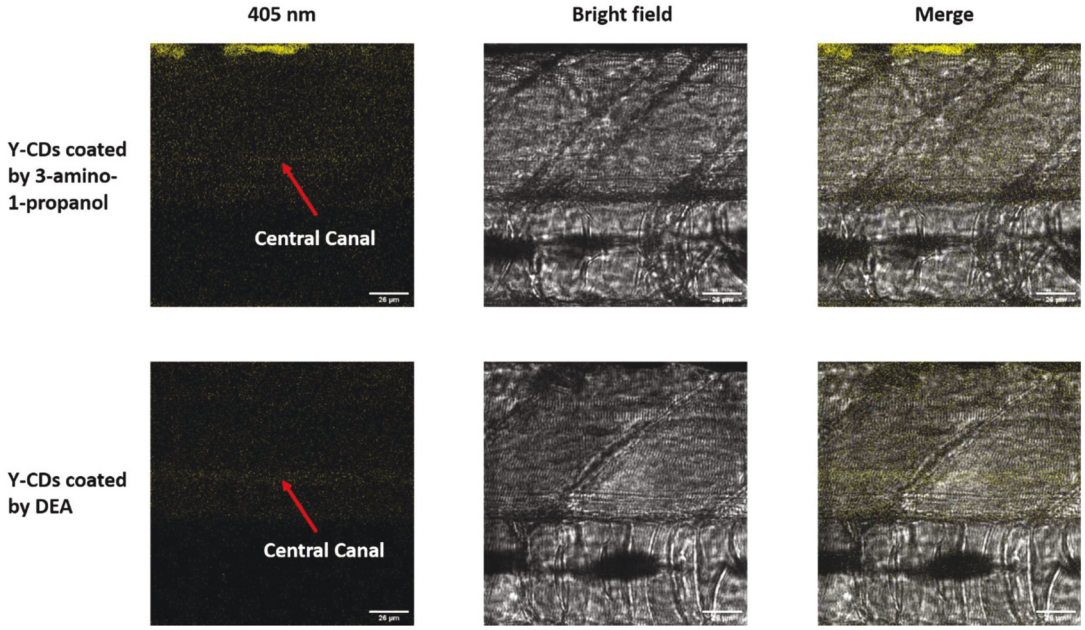

Fig. 3 Confocal images of Y-CDs coated by 3-amino-1-propanol or DEA (1.5 mg mL^{-1}) across the BBB. The red arrow indicates the central canal of spinal cord of zebrafish.

solvent effects. Furthermore, Y-CDs coated with 3-amino-1-propanol or DEA were intravascularly injected into the heart of 5-day wild-type zebrafish (number of zebrafish applied: 6). Under the excitation of 405 nm, the yellow fluorescence is clearly observed in the central canal of spinal cord (Fig. 3), which suggests that Y-CDs with both coatings crossed the BBB. Therefore, even though Y-CDs were conjugated with two hydrophilic molecules, it didn't change the amphiphilicity of Y-CDs, which helped deliver both molecules across the BBB and exhibited a great nanocarrier potential of Y-CDs.

Cytotoxicity test

The ability of Y-CDs to be used in biological applications was also tested by conducting *in vitro* viability assays. Both normal healthy (HEK293) and cancer (SJGBM2, CHLA200) cell lines were used to understand the cytotoxicity of Y-CDs. Y-CDs were dispersed in the same culture media of the cells for the treatment. The cells were incubated in different concentrations of Y-CDs aqueous dispersion such as 10 μM, 1 μM, 100 nM for 72 h before the cytotoxicity measurement using the MTS assay. The cell viability was averaged after three replicates of the cytotoxicity assay and compared with the viability of non-treated cells. As shown in Fig. 4, incubated in all the concentrations of Y-CDs aqueous dispersion, the viability of the treated cells was comparable to the non-treated cells. It is noteworthy to mention that even at a significantly high concentration as 10 μM, the cell viability was high and remained above 90% for both cancer (SJGBM2) and normal healthy (HEK293) cells. The only exception was that CHLA200 viability lowered about 15% at 10 μM but at lower concentrations such as 1 μM this also showed high viability. These results confirm that Y-CDs are non-toxic and can be used in biological applications.

In vitro bioimaging

With the aforementioned long-wavelength emission of Y-CDs which allow PL in the yellow region, we were intrigued to perform cellular bioimaging using these CDs. The low cytotoxicity observed and good amphiphilic characteristic shown by Y-CDs were also positive points for this. For the bioimaging we used two different cell lines: pediatric glioblastoma cell line (SJGBM2) and a non-cancer cell line which is normal human embryonic kidney cell line (HEK293). Both cell lines were initially plated on FBS coated glass coverslips treated with RPMI growth media for 48 h for the cell establishment before treating with the 50 μg ml^{-1} Y-CDs diluted media. Due to the excellent amphiphilicity of Y-CDs they were able to well disperse in the growth media itself without first diluting in water. After 24 h of Y-CDs treatment the cells were fixed and the coverslips were mounted onto microscope slides for the imaging. The imaging was performed using a confocal microscope at 488 nm excitation. Both cell types showed bright PL and the PL were mainly localized in the cytoplasm areas compared to nucleus (Fig. 5). The large nucleus of the cancer SJGBM2 cell (Fig. 5b) was clearly visible with a lower PL compared to the bright outline of the cytoplasm. This phenomena was also similar in the non-cancer kidney cell line (Fig. 5a) as well although the nucleus of these cells are smaller compared to the cancerous cells. This shows that Y-CDs possibly enter the cells through passive diffusion and concentrate inside the cytoplasm while only a small amount could enter the nucleus considering the lower PL visible from the nucleus of the cells.

Y-CDs inhibiting APP production and reducing the release of Aβ

It is of great significance to inhibit the production of both Aβ and APP because Aβ derives from the cleavage of APP by beta

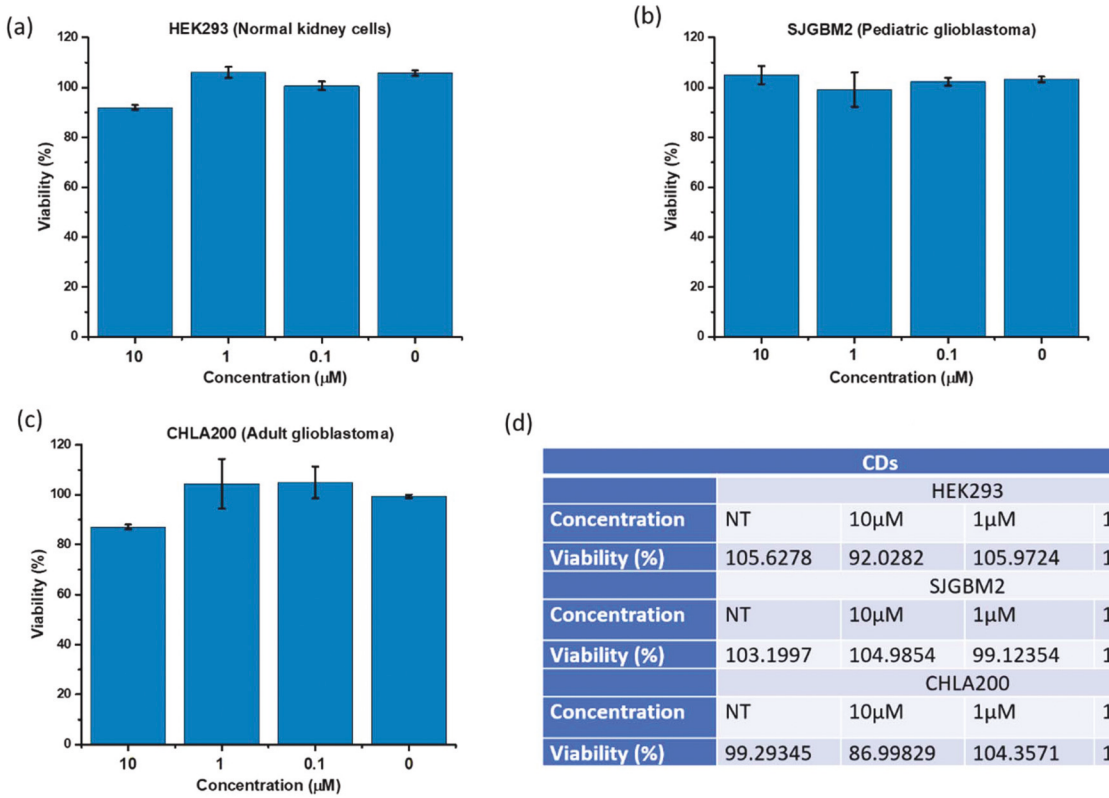

(d)

CDs				
	HEK293			
Concentration	NT	10μM	1μM	100nM
Viability (%)	105.6278	92.0282	105.9724	100.6887
	SJGBM2			
Concentration	NT	10μM	1μM	100nM
Viability (%)	103.1997	104.9854	99.12354	102.2839
	CHLA200			
Concentration	NT	10μM	1μM	100nM
Viability (%)	99.29345	86.99829	104.3571	104.8868

Fig. 4 Cytotoxicity test of Y-CDs with different cell lines: (a) normal kidney cells HEK293; (b) glioblastoma SJGBM2; (c) glioblastoma CHLA200. *NT/0 μM – nontreated (without any Y-CDs). (d) are the averaged data sets used above. Standard error was calculated and shown with each measurement of viability in the graphs above.

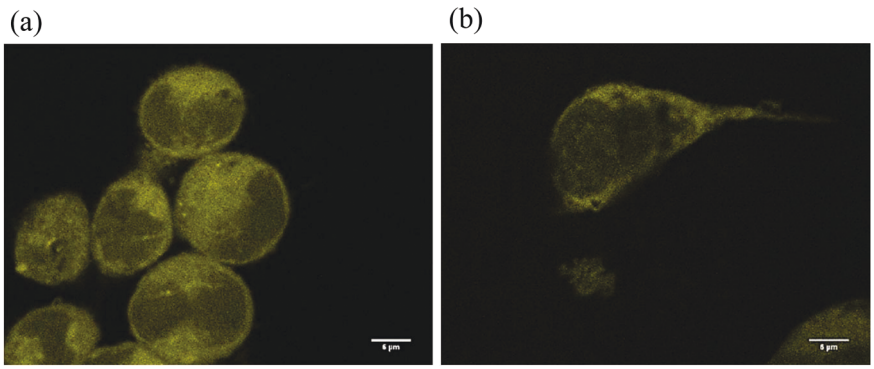

Fig. 5 *In vitro* bioimaging of (a) normal human embryonic kidney cells (HEK293) and (b) pediatric glioblastoma cell line (SJGBM2) with 24 h treatment of 50 μg ml^{-1} Y-CDs. The excitation wavelength is 488 nm.

secretase and gamma secretase. Aβ can clump into amyloid plaques which eventually will contribute to the AD. In this study, Y-CDs have revealed the ability to inhibit APP production which was assessed by an immunofluorescence analysis. In untreated cells (vehicle) there was a robust aggregation of APP (Fig. 6A, plate 1) which clearly indicated that these cells stably express human APP751. Upon treatment with Y-CDs, the expression of human APP751 was dose-dependently inhibited with the increasing concentration of Y-CDs (Fig. 6A plate 2 and Fig. 6B). Among the four concentrations used, there was a highly significant reduction at 1 and 10 μM treatment. A similar trend was also observed when the secretory Aβ levels were analyzed (Fig. 6C). Compared to the culture media from untreated cells there was a ~20% reduction in the secreted Aβ levels following the treatment with Y-CDs at 10 μM concentration. Fig. 7A depicts the cellular uptake of Y-CDs aggregates and there was no toxicity observed following CD treatments at different concentrations even at 48 h post-treatment (Fig. 7B).

In order to prevent the formation of amyloid plaque, numerous researches have been dedicated to the inhibition of

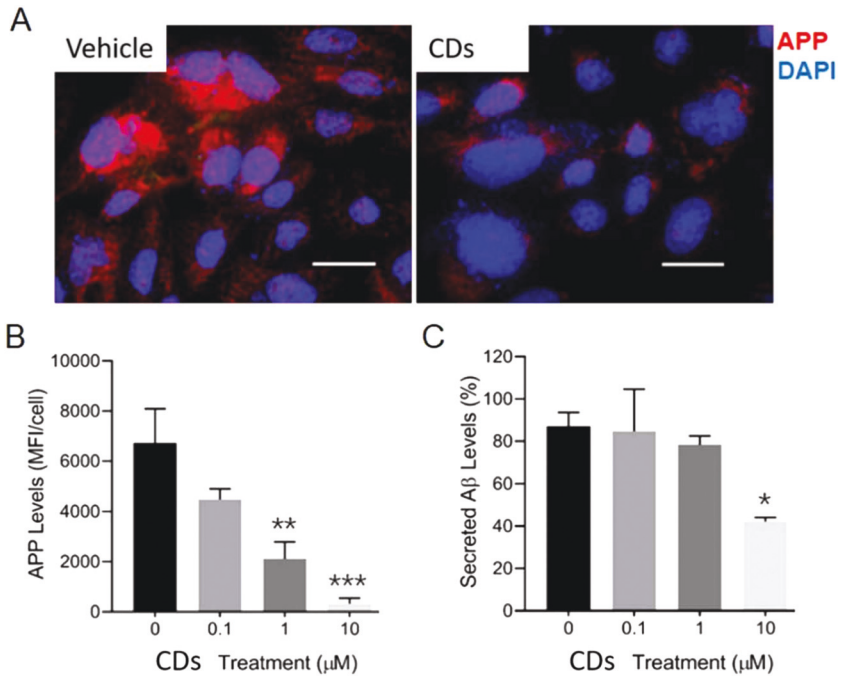

Fig. 6 *In vitro* efficacy of Y-CDs. The Chinese hamster ovary (CHO) cells that are stably overexpressing APP were incubated with 0, 0.1, 1 and 10 μM Y-CDs aqueous dispersion for 24 h. (A) Y-CDs significantly reduced APP production. Representative micrographs of CHO cells treated with vehicle and 10 μM of Y-CDs showing APP (red) and nuclei (DAPI), scale – 20 μm. The CHO cells overexpressing human APP751 were treated with Y-CDs and were fixed at 24 h and permeabilized cells were detected using APP antibody and stained with streptavidin-Alexa647. Robust APP staining was observed in vehicle treated cells compared to cells treated with 10 μM of Y-CDs. (B) Quantification of APP mean fluorescence intensity (MFI) per cell following Y-CDs treatments. The number of cells and the MFI per cell was quantified using NIH Image J software with more than 300 cells counted per treatment. (C) Quantification of the secreted β-Amyloid (Aβ) monomers in cell culture media following Y-CDs treatments. Data expressed as mean ± SEM of two independent experiments. * $P < 0.05$; ** $P < 0.01$; ***$P < 0.001$ based on the ANOVA (analysis of variance) and Tukey's *post hoc* test compared to vehicle (0 μM) control.

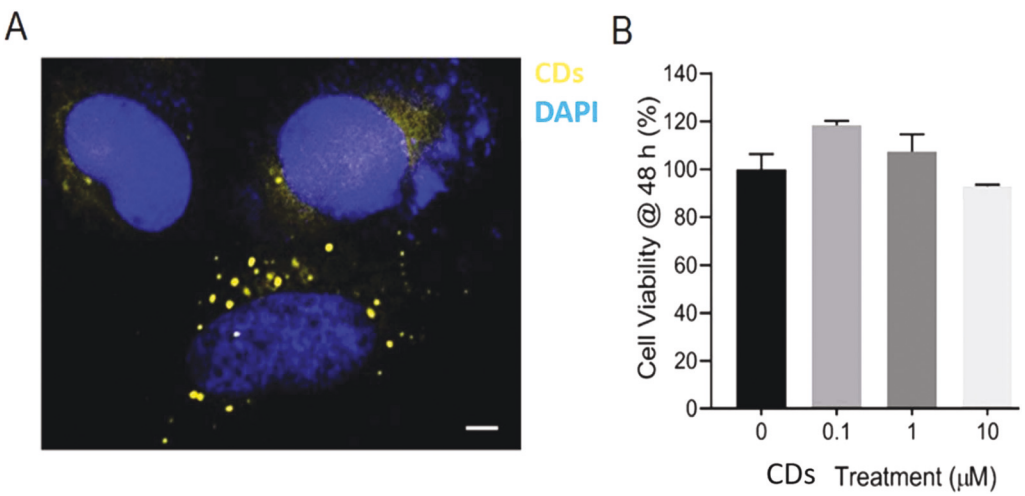

Fig. 7 Cellular uptake and *in vitro* toxicity of Y-CDs. (A) Representative micrographs of CHO cells treated with 10 μM of Y-CDs showing the fluorescence of Y-CDs (yellow) along with the nuclei (DAPI), scale – 5 μm. (B) Quantification of cell viability of CHO cells overexpressing human APP following the 48 h treatment with 0, 0.1, 1 and 10 μM of Y-CDs. Data expressed as mean ± SEM.

Aβ fibrillation. Mechanistic studies demonstrated that the inhibition occurs when Aβ monomers bind to the surfaces of the CDs with either hydrophilic or hydrophobic surface through distinct binding patterns.[17] The monomer has more contact with the hydrophilic surface. Most of the residues of monomer are able to interact with the surface of CDs through the backbone while few residues are able to interact with hydrophobic surfaces. The Aβ monomer therefore forms more

extended structures with higher flexibility on the hydrophilic surface and more compact ones on the hydrophobic surface. Moreover, previous experimental and computational studies suggested that the increased flexibility could inhibit the formation of Aβ fibrillation.[17] Thus we learnt that the inhibition of fibrillation is possible by inducing the extension of the structure and flexibility of the Aβ monomer by using hydrophilic CDs. In this study, the obtained Y-CDs demonstrated an amphiphilic characteristic. It means Y-CDs do not only have hydrophilic surface but also more hydrophobic functionalities than hydrophilic CDs. The hydrophilic surface will be beneficial for the inhibition of Aβ fibrillation while the abundant hydrophobic functionalities lead to Y-CDs across the BBB *via* passive diffusion.

In addition, in this study, different from many researchers that apply CDs to prevent established Aβ monomers from oligomerization or fibrillation,[17,53] Y-CDs were applied to inhibit the production of APP and Aβ monomers, which can eradicate the AD cause in the beginning. Furthermore, Y-CDs were used to treat Aβ as well as APP in cells instead of test tubes, which is more similar to the real CNS condition and environment. Eventually, Y-CDs exhibit great potential as nontoxic nanocarriers for drug delivery toward the CNS, proved *in vivo* to cross the BBB, and are promising inhibitors of amyloid plaques for the AD treatment in the future.

4. Conclusions

This study demonstrated that a novel type of amphiphilic Y-CDs synthesized from citric acid and *o*-phenylenediamine could cross the BBB, using zebrafish as an animal model. To investigate the mechanism that allows Y-CDs to pass the BBB, Y-CDs were systematically characterized by various spectroscopic and microscopic techniques. Y-CDs displayed a small size (3.4 nm), low zeta potential (−15.3 mV) and amphiphilicity. This led to the hypothesis that Y-CDs passed the BBB *via* passive diffusion, which was confirmed by the permeation of Y-CDs through the spinal cord of zebrafish in comparison to other CDs preparations. And the amphiphilicity of Y-CDs didn't get changed with different coatings, which benefited the delivery of coating molecules across the BBB and revealed a good nanocarrier nature. In addition, Y-CDs were also observed to cross the cell membrane and enter the cytosolic compartments, which could be exploited to monitor/modulate the intracellular activities using Y-CDs. Above all, Y-CDs were examined for toxicity in four different cell lines, which proved that Y-CDs are nontoxic. Also, Y-CDs were used to test their efficacy in cells stably overexpressing human APP751, and Y-CDs significantly inhibited the expression and secretion of Aβ. Therefore, based on these pivotal findings, this study suggests that this novel Y-CDs themselves have exhibited the excellent capability to cross the BBB and cell membrane while suppressing the production of APP and the release of Aβ. Most importantly, Y-CDs have shown the promise to be a potential drug nanocarrier for the AD treatment of *in vivo* in the future.

Conflicts of interest

The authors declare no conflict of interest.

Acknowledgements

This work was supported by National Science Foundation under the grant 011298. Also, authors gratefully acknowledge the great support from King Abdulaziz University, Kingdom of Saudi Arabia, and University of Miami, USA. Prof. Hitendra S. Chand acknowledges support from NIH grants R01DA040537 and R03DA044877, the Florida International University, Herbert Wertheim College of Medicine, and Office of Research and Economic Development Startup funds.

References

1 C. Sul-Hee, *BMB Rep.*, 2009, **42**, 467–474.
2 M. M. Mielke, P. Vemuri and W. A. Rocca, *Clin. Epidemiol.*, 2014, **6**, 37–48.
3 Alzheimer's Association, *Alzheimers Dement.*, 2015, **11**, 332–384.
4 S. Bhattacharya, C. Haertel, A. Maelicke and D. Montag, *PLoS One*, 2014, **9**, e89454–e89465.
5 S. Manoharan, G. J. Guillemin, R. S. Abiramasundari, M. M. Essa, M. Akbar and M. D. Akbar, *Oxid. Med. Cell. Longevity*, 2016, **2016**, 15–29.
6 K. Buerger, M. Ewers, T. Pirttilä, R. Zinkowski, I. Alafuzoff, S. J. Teipel, J. DeBernardis, D. Kerkman, C. McCulloch, H. Soininen and H. Hampel, *Brain*, 2006, **129**, 3035–3041.
7 C. R. Harrington, *Neuroimaging Clin. N. Am.*, 2012, **22**, 11–22.
8 P. Shi, M. Li, J. Ren and X. Qu, *Adv. Funct. Mater.*, 2013, **23**, 5412–5419.
9 R. Daneman and A. Prat, *Cold Spring Harbor Perspect. Biol.*, 2015, **7**, a020412–a020435.
10 Y. Zhou, Z. Peng, E. S. Seven and R. M. Leblanc, *J. Controlled Release*, 2018, **270**, 290–303.
11 J. Barar, M. A. Rafi, M. M. Pourseif and Y. Omidi, *BioImpacts*, 2016, **6**, 225–248.
12 C. Greene and M. Campbell, *Tissue Barriers*, 2016, **4**, e1138017–e1138026.
13 R. Singh and J. W. Lillard, *Exp. Mol. Pathol.*, 2009, **86**, 215–223.
14 K. J. Mintz, Y. Zhou and R. M. Leblanc, *Nanoscale*, 2019, **11**, 4634–4652.
15 Y. Zhou, E. M. Zahran, B. A. Quiroga, J. Perez, K. J. Mintz, Z. Peng, P. Y. Liyanage, R. R. Pandey, C. C. Chusuei and R. M. Leblanc, *Appl. Catal., B*, 2019, **248**, 157–166.
16 S. Li, L. Wang, C. C. Chusuei, V. M. Suarez, P. L. Blackwelder, M. Micic, J. Orbulescu and R. M. Leblanc, *Chem. Mater.*, 2015, **27**, 1764–1771.

17 X. Han, Z. Jing, W. Wu, B. Zou, Z. Peng, P. Ren, A. Wikramanayake, Z. Lu and R. M. Leblanc, *Nanoscale*, 2017, **9**, 12862–12866.
18 K. J. Mintz, G. Mercado, Y. Zhou, Y. Ji, S. D. Hettiarachchi, P. Y. Liyanage, R. R. Pandey, C. C. Chusuei, J. Dallman and R. M. Leblanc, *Colloids Surf., B*, 2019, **176**, 488–493.
19 K. Jiang, X. Feng, X. Gao, Y. Wang, C. Cai, Z. Li and H. Lin, *Nanomaterials*, 2019, **9**, 529.
20 T. Zhang, J. Zhu, Y. Zhai, H. Wang, X. Bai, B. Dong, H. Wang and H. Song, *Nanoscale*, 2017, **9**, 13042–13051.
21 H. Ding, J.-S. Wei, P. Zhang, Z.-Y. Zhou, Q.-Y. Gao and H.-M. Xiong, *Small*, 2018, **14**, 1800612–1800621.
22 A. V. Kalueff, A. M. Stewart and R. Gerlai, *Trends Pharmacol. Sci.*, 2014, **35**, 63–75.
23 S. Li, Z. Peng, J. Dallman, J. Baker, A. M. Othman, P. L. Blackwelder and R. M. Leblanc, *Colloids Surf., B*, 2016, **145**, 251–256.
24 A. Avdesh, M. Chen, M. T. Martin-Iverson, A. Mondal, D. Ong, S. Rainey-Smith, K. Taddei, M. Lardelli, D. M. Groth, G. Verdile and R. N. Martins, *J. Visualized Exp.*, 2012, **69**, e4196–e4203.
25 J. R. Meyers, *Curr. Protoc.*, 2018, **16**, e19–e44.
26 Y. Zhou, P. Y. Liyanage, D. L. Geleroff, Z. Peng, K. J. Mintz, S. D. Hettiarachchi, R. R. Pandey, C. C. Chusuei, P. L. Blackwelder and R. M. Leblanc, *ChemPhysChem*, 2018, **19**, 2589–2597.
27 Y. Zhou, A. Desserre, S. K. Sharma, S. Li, M. H. Marksberry, C. C. Chusuei, P. L. Blackwelder and R. M. Leblanc, *ChemPhysChem*, 2017, **18**, 890–897.
28 Z. Ma, H. Ming, H. Huang, Y. Liu and Z. Kang, *New J. Chem.*, 2012, **36**, 861–864.
29 A. C. Vandaele, C. Hermans, P. C. Simon, M. Van Roozendael, J. M. Guilmot, M. Carleer and R. Colin, *J. Atmos. Chem.*, 1996, **25**, 289–305.
30 Y. Zhou, K. J. Mintz, C. Y. Oztan, S. D. Hettiarachchi, Z. Peng, E. S. Seven, P. Y. Liyanage, S. De La Torre, E. Celik and R. M. Leblanc, *Polymers*, 2018, **10**, 921–932.
31 Y. Guo, D. Wang, X. Liu, X. Wang, W. Liu and W. Qin, *New J. Chem.*, 2014, **38**, 5861–5867.
32 U. Langheinrich, *Bioessays*, 2003, **25**, 904–912.
33 L. A. Rudner, K. H. Brown, K. P. Dobrinski, D. F. Bradley, M. I. Garcia, A. C. H. Smith, J. M. Downie, N. D. Meeker, A. T. Look, J. R. Downing, A. Gutierrez, C. G. Mullighan, J. D. Schiffman, C. Lee, N. S. Trede and J. K. Frazer, *Oncogene*, 2011, **30**, 4289–4296.
34 P. Outtandy, C. Russell, R. Kleta and D. Bockenhauer, *Pediatr. Nephrol.*, 2019, **34**, 751–762.
35 Y. Xi, S. Noble and M. Ekker, *Curr. Neurol. Neurosci. Rep.*, 2011, **11**, 274–282.
36 S. Saleem and R. R. Kannan, *Cell Death Discovery*, 2018, **4**, 45–57.
37 D. G. Howe, Y. M. Bradford, A. Eagle, D. Fashena, K. Frazer, P. Kalita, P. Mani, R. Martin, S. T. Moxon, H. Paddock, C. Pich, S. Ramachandran, L. Ruzicka, K. Schaper, X. Shao, A. Singer, S. Toro, C. Van Slyke and M. Westerfield, *Nucleic Acids Res.*, 2017, **45**, D758–D768.
38 C. Santoriello and L. I. Zon, *J. Clin. Invest.*, 2012, **122**, 2337–2343.
39 D. Kokel, J. Bryan, C. Laggner, R. White, C. Y. J. Cheung, R. Mateus, D. Healey, S. Kim, A. A. Werdich, S. J. Haggarty, C. A. MacRae, B. Shoichet and R. T. Peterson, *Nat. Chem. Biol.*, 2010, **6**, 231–237.
40 J. Rihel, D. A. Prober, A. Arvanites, K. Lam, S. Zimmerman, S. Jang, S. J. Haggarty, D. Kokel, L. L. Rubin, R. T. Peterson and A. F. Schier, *Science*, 2010, **327**, 348–351.
41 I. Javed, G. Peng, Y. Xing, T. Yu, M. Zhao, A. Kakinen, A. Faridi, C. L. Parish, F. Ding, T. P. Davis, P. C. Ke and S. Lin, *Nat. Commun.*, 2019, **10**, 3780–3793.
42 I. Javed, T. Yu, G. Peng, A. Sánchez-Ferrer, A. Faridi, A. Kakinen, M. Zhao, R. Mezzenga, T. P. Davis, S. Lin and P. C. Ke, *Nano Lett.*, 2018, **18**, 5797–5804.
43 M. Wang, Y. Sun, X. Cao, G. Peng, I. Javed, A. Kakinen, T. P. Davis, S. Lin, J. Liu, F. Ding and P. C. Ke, *Nanoscale*, 2018, **10**, 19995–20006.
44 Y.-E. L. Koo, G. R. Reddy, M. Bhojani, R. Schneider, M. A. Philbert, A. Rehemtulla, B. D. Ross and R. Kopelman, *Adv. Drug Delivery Rev.*, 2006, **58**, 1556–1577.
45 M. K. Gumerlock, B. D. Belshe, R. Madsen and C. Watts, *J. Neuro-Oncol.*, 1992, **12**, 33–46.
46 S.-K. Wu, P.-C. Chu, W.-Y. Chai, S.-T. Kang, C.-H. Tsai, C.-H. Fan, C.-K. Yeh and H.-L. Liu, *Sci. Rep.*, 2017, **7**, 46689–46699.
47 P.-C. Chu, W.-Y. Chai, C.-H. Tsai, S.-T. Kang, C.-K. Yeh and H.-L. Liu, *Sci. Rep.*, 2016, **6**, 33264–33276.
48 R. K. Upadhyay, *BioMed Res. Int.*, 2014, **2014**, 869269–869305.
49 E. Nance, K. Timbie, G. W. Miller, J. Song, C. Louttit, A. L. Klibanov, T.-Y. Shih, G. Swaminathan, R. J. Tamargo, G. F. Woodworth, J. Hanes and R. J. Price, *J. Controlled Release*, 2014, **189**, 123–132.
50 T.-T. Zhang, W. Li, G. Meng, P. Wang and W. Liao, *Biomater. Sci.*, 2016, **4**, 219–229.
51 Y. Zhou, K. J. Mintz, S. K. Sharma and R. M. Leblanc, *Langmuir*, 2019, **35**, 9115–9132.
52 K. J. Mintz, B. Guerrero and R. M. Leblanc, *J. Phys. Chem. C*, 2018, **122**, 29507–29515.
53 R. Malishev, E. Arad, S. K. Bhunia, S. Shaham-Niv, S. Kolusheva, E. Gazit and R. Jelinek, *Chem. Commun.*, 2018, **54**, 7762–7765.